Electronic Supplementary Information

Actuation of Bilayer Hydrogels via a Cross-Stimuli Chemical Reaction Network

Zhongrui Wang[a], Yongzheng Xing[a], Yuwen Meng[a,] and Xu Wang[a,b,*]*

[a]National Engineering Research Center for Colloidal Materials, School of Chemistry and Chemical Engineering, Shandong University, Jinan, Shandong 250100, People's Republic of China

[b]Intelligent Chemical Engineering Center, Hong Kong Research Institute of Shandong University, Hong Kong SAR, 999077, People's Republic of China

*Corresponding authors: yuwen.meng@sdu.edu.cn (Y. M.); wangxu@sdu.edu.cn (X. W.)

1. Experimental Section

1.1. Materials

2-Hydroxyethyl methacrylate (HEMA), *N*-isopropylacrylamide (NIPAM), methylene-bis-acrylamide (MBAA), glycine, and 2-hydroxy-4′-(2-hydroxyethoxy)-2-methylpropiophenone (Irgacure 2959) were purchased from Aladdin Biochemical Technology Co., Ltd. (Shanghai, China). Poly (ethylene glycol) (M_n = 6000 g mol^{-1}), ammonium carbonate ($(NH_4)_2CO_3$), sodium hydroxide, and [2-(methacryloyloxy)ethyl]dimethyl-(3-sulfopropyl)ammonium hydroxide (SBMA) were purchased from Macklin Biochemical Technology Co., Ltd. (Shanghai, China). Potassium dihydrogen phosphate and dipotassium hydrogen phosphate were purchased from Sinopharm Chemical Reagent Co., Ltd. (Shanghai, China). NIPAM was recrystallized before use. Deionized water was used for all the experiments.

1.2. Methods

1.2.1. Fabrication of thermo-responsive and ionic strength-responsive hydrogels

For thermo-responsive hydrogels, a prepolymer solution was prepared by dissolving NIPAM, PEG, MBAA, and Irgacure 2959 in deionized water at concentrations detailed in Table S1 (ESI). Following thorough mixing, 0.5 mL of the solution was dispensed into each well of a 24-well plate. The solutions were then photopolymerized under UV irradiation (365 nm, 40 W) for 20 min. The resulting hydrogels were carefully demolded and subjected to subsequent soaking. Thorough washing is required prior to the soaking process to remove unreacted monomers.

The preparation of ionic strength-responsive hydrogels followed a procedure analogous

to that described for thermo-responsive hydrogels, except that the prepolymer solution was substituted with the composition and ratios specified in Table S2 (ESI); all other parameters remained unchanged.

1.2.2. Determination of water contents

The water content (C_w) of the hydrogels was calculated from the weight difference before and after freeze-drying, which was presented as follows:

$$C_W = \frac{W_s - W_d}{W_s} \times 100\% \quad (1)$$

where W_s (unit: g) and W_d (unit: g) are the weights of the hydrogels before (at swelling equilibrium) and after freeze-drying, respectively.

1.2.3. Determination of swelling ratios

The swelling ratio (*SR*) of the hydrogels was measured using the gravimetric method. The *SR* value was calculated by the following equation:

$$SR = \frac{W_e}{W_i} \quad (2)$$

where W_e (unit: g) is the weight of swollen hydrogels at equilibrium in different solutions, and W_i (unit: g) is the weight of initial hydrogels.

1.2.4. Preparation of bilayer hydrogels

Bilayer hydrogels were fabricated via a layer-by-layer photopolymerization technique. The lower layer, consisting of P(SBMA-*co*-HEMA)$_{0.3}$, was prepared by adding 3 mL of the corresponding prepolymer solution to a rectangular silicone mold and allowing it to polymerize completely. Following the formation of the lower layer, 3 mL of a PNIPAM$_{1.0}$/PEG prepolymer solution was added to form the upper layer. The resulting bilayer hydrogels were then trimmed

to dimensions of 4 cm × 0.5 cm × 0.7 cm (length × width × height).

1.2.5. Measurement of the curvature of bilayer hydrogels

The bending behavior of the bilayer hydrogels under varying conditions was quantified by measuring curvatures, following established methods in the literature.[1] The curvature was defined as zero for the unbent, initial state. The curvature was assigned a positive value when the hydrogel bent towards the $PNIPAM_{1.0}$/PEG side and a negative value when bending occurred towards the $P(SBMA\text{-}co\text{-}HEMA)_{0.3}$ side.

1.2.6. Characterizations

Fourier-transform infrared (FTIR) spectroscopy was performed on freeze-dried hydrogel samples using a Bruker TENSOR II spectrometer. The optical transmittance of the hydrogels was measured across a specified wavelength range using a UV-vis spectrophotometer (Hitachi, U-3900H). The rheological properties of the hydrogel samples were characterized using an Anton Paar MCR302 rheometer, employing PP25 geometry and a frequency sweep test. The electrical conductivity of the solutions was determined using a conductivity meter (Leici, DDSJ-308F). Optical micrographs of the interface of the bilayer hydrogel were obtained using an MP41 microscope (Guangzhou Micro-shot Technology Co., Ltd.) in a reflection mode. The morphology of the freeze-dried hydrogels was investigated by scanning electron microscopy using a Hitachi SU8010 microscope. Prior to imaging, the hydrogel samples were pre-frozen at -20 °C, lyophilized, and sputter-coated with platinum to enhance conductivity.

2. Supporting tables

Table S1. Compositions of PNIPAM/PEG hydrogels.

hydrogel	c(NIPAM)/M	c(PEG)/(g/mL)	c(MBAA)/M	c(Irgacure 2959)
$PNIPAM_{0.25}$/PEG	0.25	0.1	0.02	0.1
$PNIPAM_{0.5}$/PEG	0.5	0.1	0.02	0.1
$PNIPAM_{1.0}$/PEG	1.0	0.1	0.02	0.1
$PNIPAM_{1.5}$/PEG	1.5	0.1	0.02	0.1
$PNIPAM_{2.0}$/PEG	2.0	0.1	0.02	0.1

Table S2. Compositions of P(SBMA-*co*-HEMA) hydrogels.

hydrogel	c(SBMA)/M	c(HEMA)/M	c(MBAA)/M	c(Irgacure 2959)
P(SBMA-*co*-HEMA)$_{0.05}$	0.05	2.15	0.02	0.1
P(SBMA-*co*-HEMA)$_{0.1}$	0.1	2.1	0.02	0.1
P(SBMA-*co*-HEMA)$_{0.2}$	0.2	2.0	0.02	0.1
P(SBMA-*co*-HEMA)$_{0.3}$	0.3	1.9	0.02	0.1

3. Supporting figures

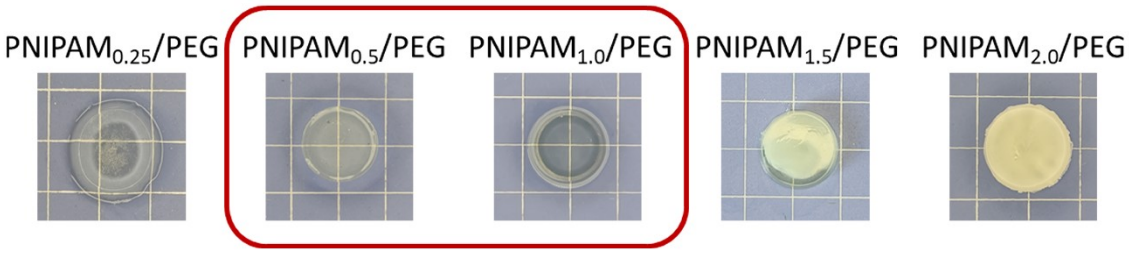

Fig. S1. Photographs showing the five hydrogels obtained after polymerization, demonstrating successful gel formation.

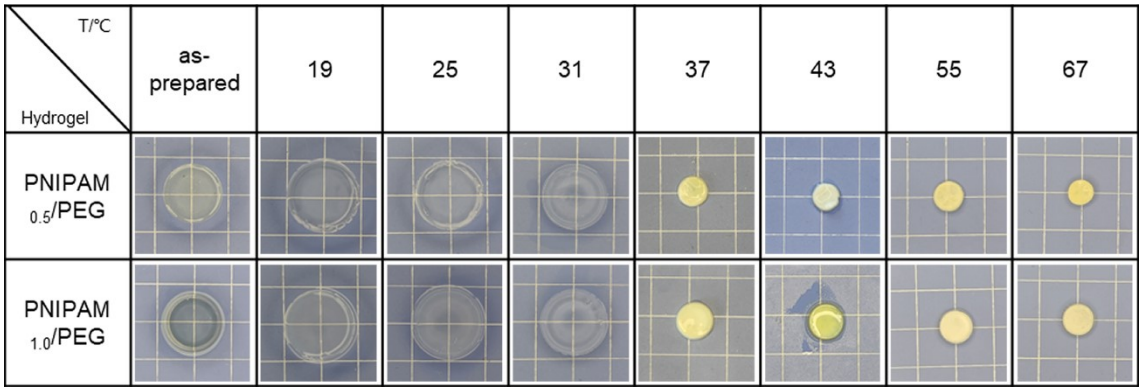

Fig. S2. Photographs of $PNIPAM_{0.5}$/PEG and $PNIPAM_{1.0}$/PEG hydrogels at various temperatures, illustrating their thermo-responsive behavior.

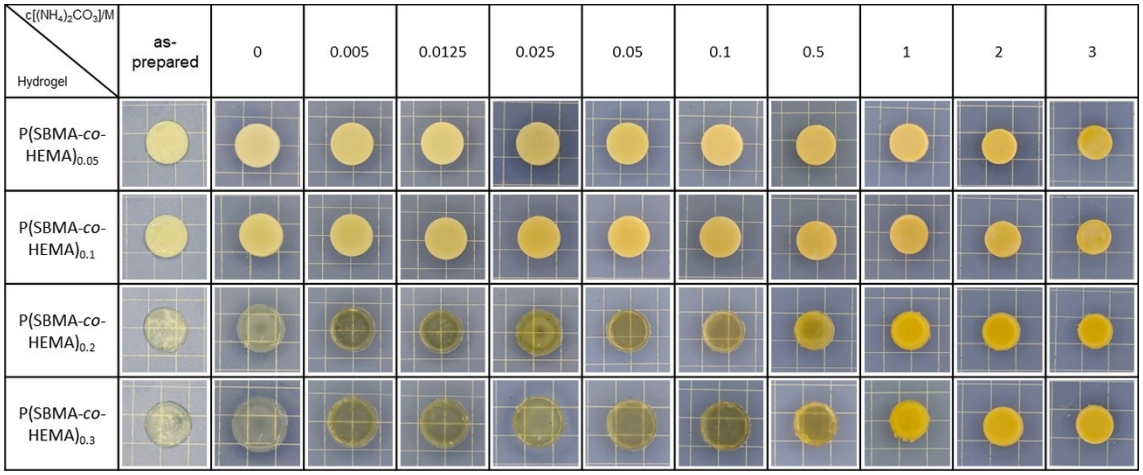

Fig. S3. Photographs illustrating the swelling behavior of P(SBMA-*co*-HEMA) hydrogels after reaching equilibrium in $(NH_4)_2CO_3$ solutions of varying concentrations.

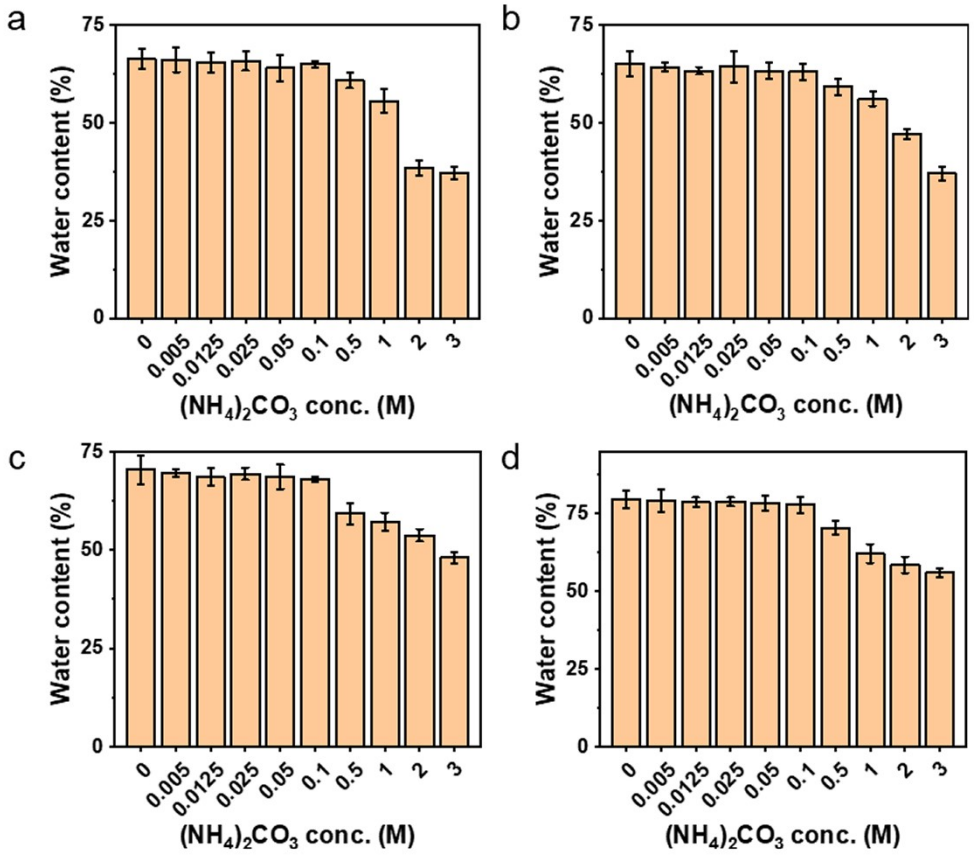

Fig. S4. Equilibrium water contents of (a) P(SBMA-*co*-HEMA)$_{0.05}$, (b) P(SBMA-*co*-HEMA)$_{0.1}$, (c) P(SBMA-*co*-HEMA)$_{0.2}$, and (d) P(SBMA-*co*-HEMA)$_{0.3}$ hydrogels after swelling in varying concentrations of $(NH_4)_2CO_3$.

pH responsiveness of P(SBMA-*co*-HEMA)$_{0.3}$

Initial pH measurements of 0 M and 3 M $(NH_4)_2CO_3$ solutions revealed an increase from pH 6.9 to 9.7 (Fig. S5a), attributable to the inherent alkalinity of dissolved $(NH_4)_2CO_3$. Subsequent immersion of P(SBMA-co-HEMA)$_{0.3}$ hydrogels in 0.1 M phosphate buffer (pH 6.9) and 0.1 M glycine-sodium hydroxide buffer (pH 9.7) demonstrated slight hydrogel swelling in the pH 9.7 buffer, visually documented in Fig. S5b (swelling ratio = 1.29, Fig. S5c). This swelling stems from enhanced deprotonation of SBMA's sulfonate groups under alkaline conditions. Critically, while swelling occurred at pH 9.7, contraction was observed in 3 M $(NH_4)_2CO_3$ solution (swelling ratio = 0.61), confirming that the anti-polyelectrolyte effect predominates over pH-mediated swelling influences.

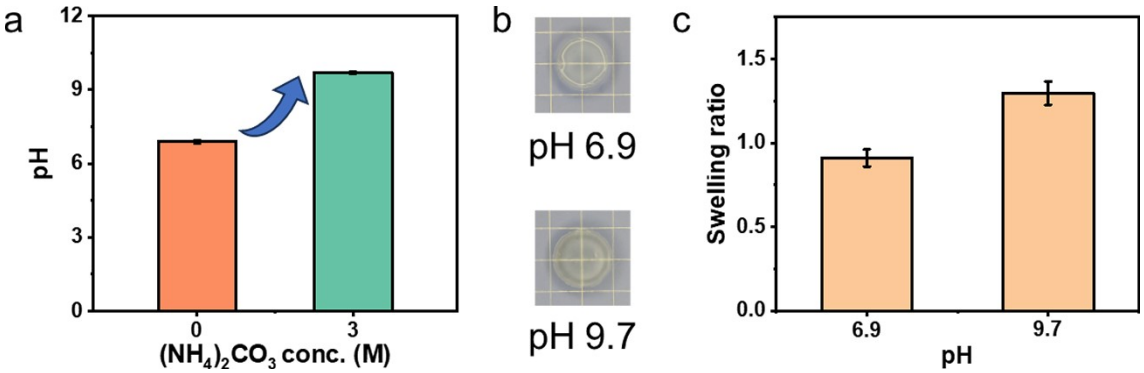

Fig. S5. Swelling behavior of P(SBMA-co-HEMA)$_{0.3}$ hydrogels under varying pH conditions. (a) pH values measured for $(NH_4)_2CO_3$ solutions at different concentrations; (b) Photographs of fully swollen P(SBMA-co-HEMA)$_{0.3}$ hydrogels in pH-buffered solutions; (c) Swelling ratios of P(SBMA-co-HEMA)$_{0.3}$ hydrogels after equilibration in pH-buffered solutions.

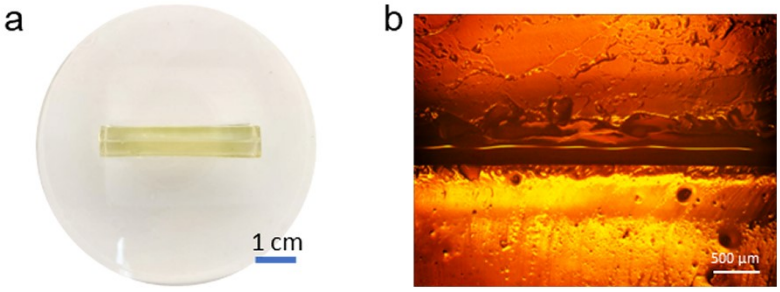

Fig. S6. (a) Digital photograph and (b) optical microscopy image of the bilayer hydrogel composed of $PNIPAM_{1.0}$/PEG (upper layer) and $P(SBMA\text{-}co\text{-}HEMA)_{0.3}$ (lower layer).

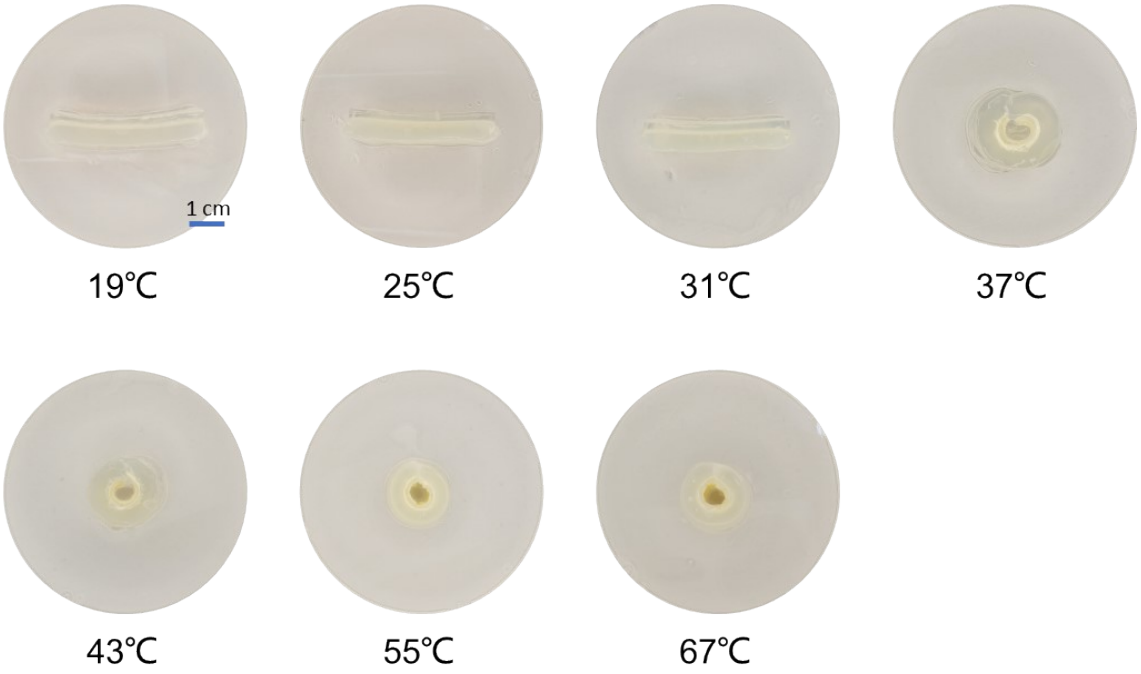

Fig. S7. Photographs illustrating the temperature-dependent swelling behavior of PNPS after reaching equilibrium at various temperatures.

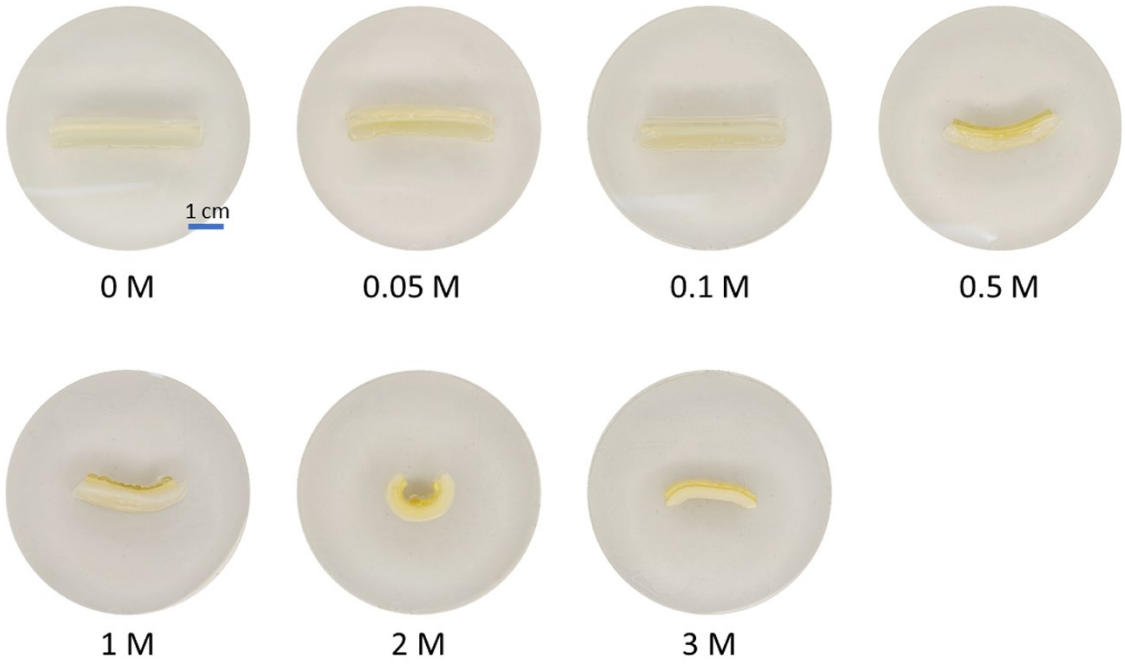

Fig. S8. Photographs illustrating the swelling behavior of PNPS in $(NH_4)_2CO_3$ solutions of varying concentrations after reaching equilibrium.

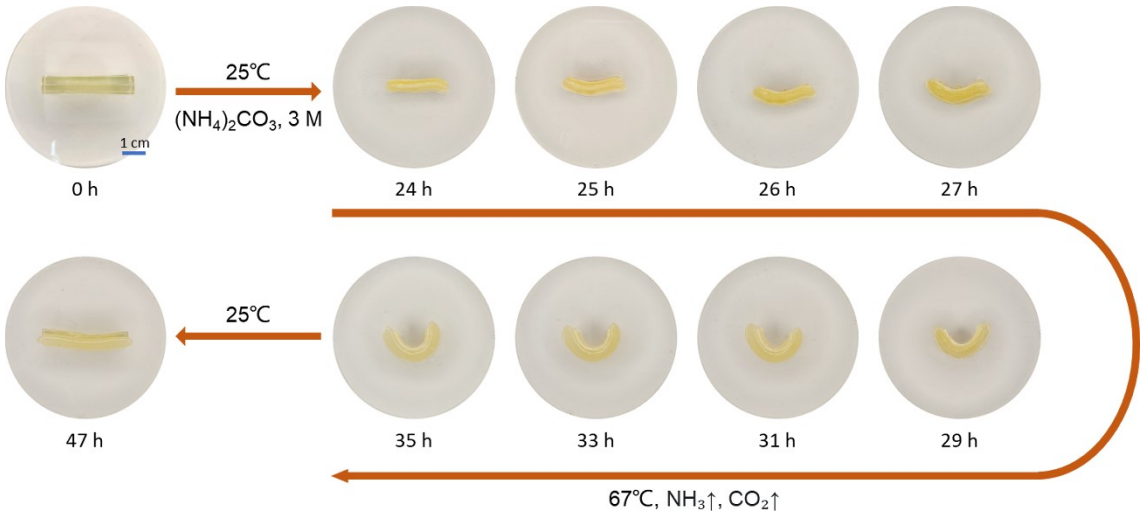

Fig. S9. Photographic representation of the actuation process of PNPS regulated by a dynamic chemical reaction network.

Effect of thickness on PNPS performance

We synthesized PNPS with varying thickness ratios and subjected them to different environments, as shown in Fig. S10. At 67°C, both PNPS samples bent toward the $PNIPAM_{1.0}$/PEG side due to its contraction. Notably, in 3 M $(NH_4)_2CO_3$ solution, the PNPS bent toward the thinner layer. This demonstrates that PNPS bending is governed not only by swelling ratio but also by water content.

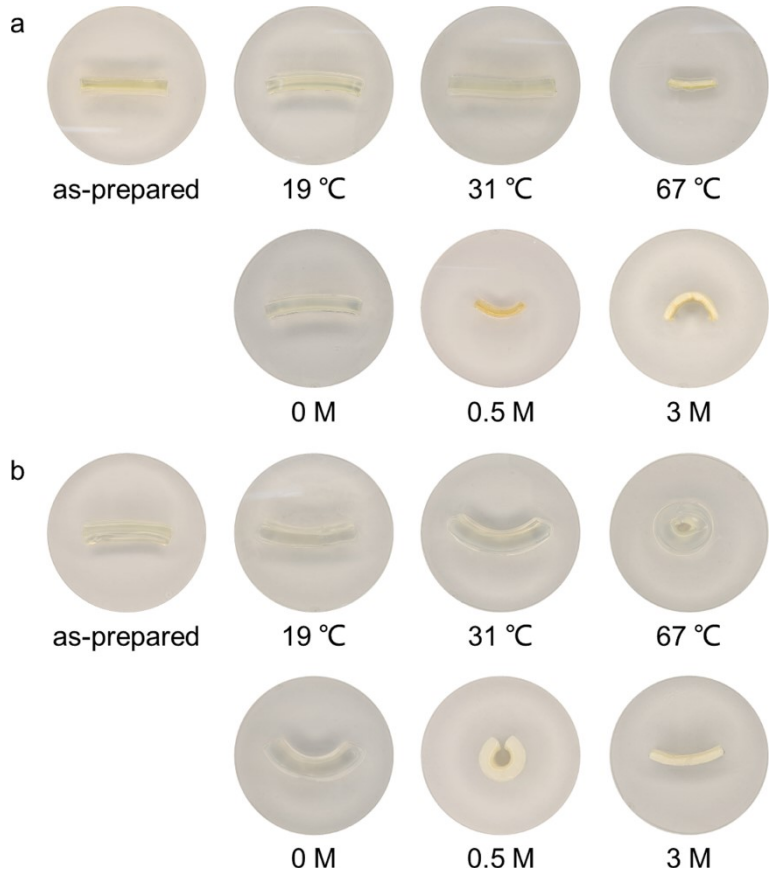

Fig. S10. Photographs of fabricated PNPS with varying thickness ratios and their bending behaviors under different environmental stimuli. (a) Thickness ratio of $PNIPAM_{1.0}$/PEG to $P(SBMA\text{-}co\text{-}HEMA)_{0.3}$ = 3:1; (b) Thickness ratio of $PNIPAM_{1.0}$/PEG to $P(SBMA\text{-}co\text{-}HEMA)_{0.3}$ = 1:3.

Cyclic actuation behavior of PNPS

We conducted four cyclic experiments on PNPS as illustrated in Fig. S9, with results presented in Fig. S11. During the first two cycles, PNPS exhibited normal behavior. However, in the third and fourth cycles, the PNPS failed to return to zero curvature even under 0 M, 25°C conditions. This irreversible deformation stems from partial configurational fixation of PNIPAM polymer chains during repeated swelling-deswelling cycles.

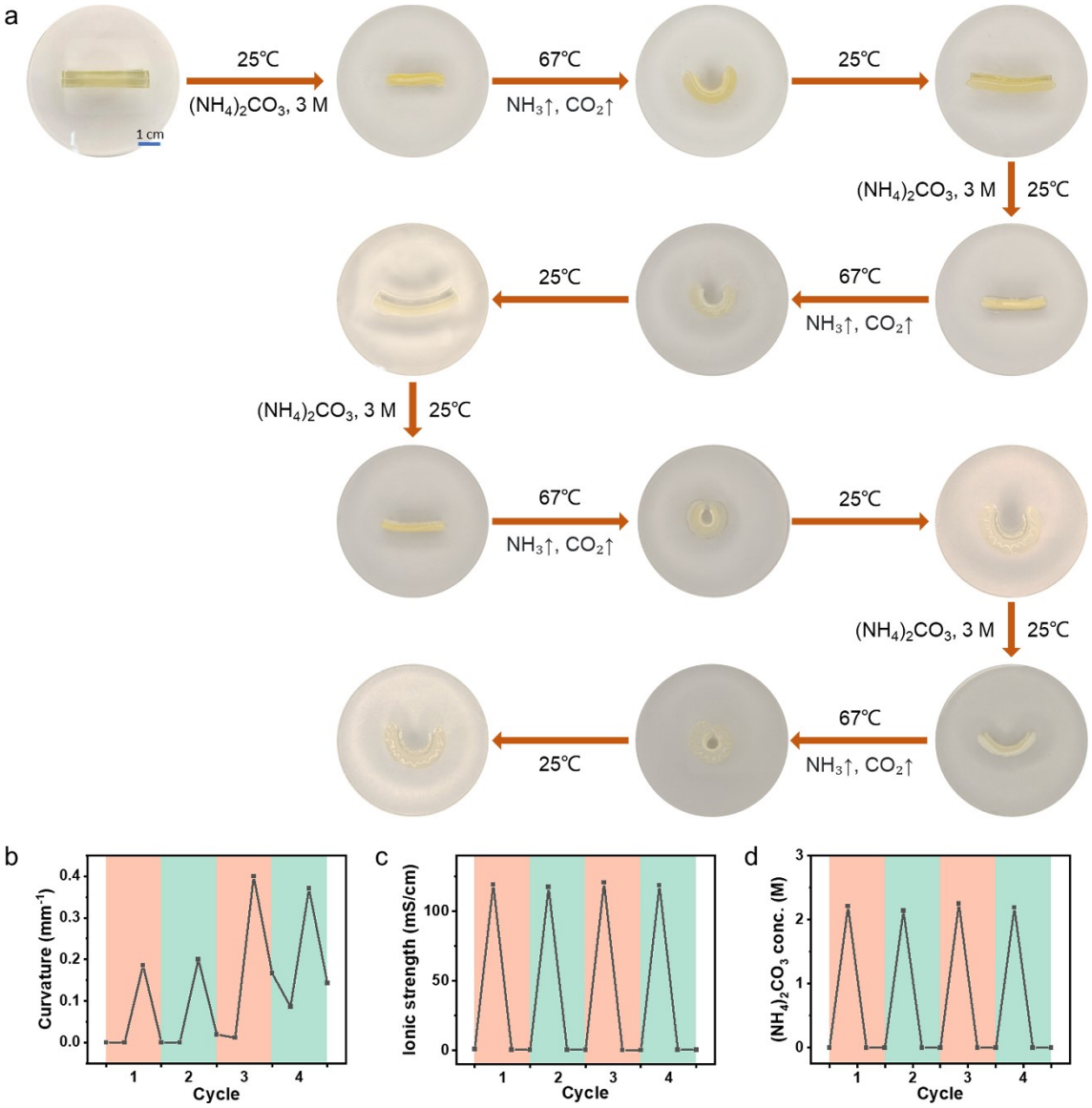

Fig. S11. Cyclic performance analysis of PNPS. (a) Photographs during four actuation cycles; (b) Curvature changes over four actuation cycles; (c) Ionic strength variation of the aqueous solution during cycling; (d) Concentration changes of $(NH_4)_2CO_3$ in solution during cycling.

References

1.X. Wang, H. Huang, H. Liu, F. Rehfeldt, X. Wang and K. Zhang, *Macromol. Chem. Phys.*, 2019, **220**, 1800562.